Excitation energies and line strengths in the Mg isoelectronic sequence*

K. T. Cheng† and W. R. Johnson
Department of Physics, University of Notre Dame, Notre Dame, Indiana 46556
(Received 16 February 1977)

Excitation energies and line strengths for the low-lying states of ions in the Mg isoelectronic sequence are studied using relativistic multiconfiguration Hartree-Fock techniques. Line strengths for all possible electric dipole transitions between these low-lying states are calculated in both the length gauge and in the velocity gauge along the sequence from Mg to U^{+80}, and the results show good agreement between these two forms of line strength for all cases considered. At low Z, the results of the present work are in good agreement with other recent theoretical calculations. The results of this work are expected to give accurate excitation energies and line strengths at high Z as well since relativistic effects are treated nonperturbatively.

I. INTRODUCTION

Theoretical studies of the line strengths for highly stripped ions are of current interest because of the usefulness of these data in astrophysical observations,[1] for plasma diagnostics in controlled thermonuclear reactions,[2] and in laboratory beam-foil experiments.[3] The main difficulty associated with these theoretical studies is that one has to deal with electron-electron correlation effects; furthermore, relativistic corrections become more and more important with increasing Z along an isoelectronic sequence, so that the usual perturbative treatment of relativistic effects is not suitable.

Recently, several fully relativistic studies of oscillator strengths have been reported for various isoelectronic sequences: the Li and Be sequences using relativistic multiconfiguration Hartree-Fock (MCHF) techniques,[4,5,6] the He, Be, and Mg sequences using the relativistic random-phase approximation (RRPA),[7,8,9] and the Mg sequence using a parametric potential.[10] For the Mg sequence, there is also the study using the superposition-of-configurations (SOC) technique with relativistic effects being treated in Pauli's approximation,[11] as well as nonrelativistic studies using a model potential[12] and the time-dependent Hartree-Fock (TDHF) method.[13]

The RRPA technique is suitable for the study of line strength at high Z. However, this method is at present confined to the studies of excitations of a single valence electron from the ground state in closed shell systems. States dominated by two-electron excitations, for example, cannot be treated in RRPA calculations. The alternative SOC and parametric potential methods do not suffer from the restriction to single-electron excitations. However, a large number of configurations is usually required to achieve good accuracy, and the quality of these studies is thus difficult to assess.

The MCHF calculations utilize a variational principle in choosing an optimum set of single-particle wave functions and, therefore, relatively few configurations are required to give accurate energy values. Furthermore, the MCHF technique provides an unambiguous way of identifying the low-lying energy levels and thus makes possible studies of systematic trends of line strengths along the entire isoelectronic sequence. To illustrate the utility of the MCHF technique, we present here a systematic study of the excitation energies and line strengths for the low-lying states of ions in the Mg isoelectronic sequence. Specifically, a set of low-lying states is generated throughout the sequence, and all possible electric dipole transitions between these states are studied in both the length gauge and the velocity gauge from Mg to U^{+80}. In the following section, we discuss the general procedure for calculations in the MCHF scheme, then in Secs. III and IV, we present and discuss our results in detail.

II. THEORY

A. Energy levels

In relativistic theory, energy levels are characterized by the total angular momentum J and the parity π. States with the same J and π are further classified by the ordering of their energies. For Mg-like ions, there are two valence electrons in the M shell, and possible energy levels are those with either even or odd parity and with $J = 0, 1, 2, \ldots$, etc.

In our present calculation, multiconfiguration wave functions are used for the ground state as well as for the other low-lying excited states. A state $|jm\rangle$ with definite parity π and angular momentum j is written as a linear combination of wave functions with different electronic configurations:

$$|jm\rangle = \sum_i c_i |(a_i b_i) jm\rangle , \tag{1}$$

TABLE I. Two electron configurations included in the present calculation are listed for each value of π and J, together with spectroscopic designations of the lowest two eigenstates.

Parity	J	Configuration	Eigenstates First	Eigenstates Second
Even	0	$3s^2, 3p_-^2, 3p_+^2, 3d_-^2, 3d_+^2$	$^1S_0$	$^3P_0$
	1	$3p_-3p_+, 3s3d_-, 3d_-3d_+$	$^3P_1$	···
	2	$3p_+^2, 3p_-3p_+, 3s3d_-, 3s3d_+, 3d_-^2, 3d_+^2, 3d_-3d_+$	$^1D_2$	$^3P_2$
Odd	0	$3s3p_-, 3p_+3d_-$	$^3P_0$	···
	1	$3s3p_-, 3s3p_+, 3p_-3d_-, 3p_+3d_-, 3p_+3d_+$	$^3P_1$	$^1P_1$
	2	$3s3p_+, 3p_-3d_-, 3p_-3d_+, 3p_+3d_-, 3p_+3d_+$	$^3P_2$	···

where (a_ib_i) denotes a configuration of the two valence electrons, and c_i is the corresponding weighting factor. In Eq. (1), $|(ab)jm\rangle$ are antisymmetric wave functions of the total angular momentum j constructed from Slater determinants of single-particle orbitals $|j_am_aj_bm_b\rangle$ as

$$|(ab)jm\rangle = \sum_{m_am_b} C(j_aj_bj; m_am_bm)|j_am_aj_bm_b\rangle. \quad (2)$$

In constructing the wave functions $|jm\rangle$ in Eq. (1), we have confined ourselves to those configurations within the same complex, i.e., having the same principal quantum number n (in our present case, $n=3$). This, however, is not a serious restriction. As we shall show in the next section, the values of the energy levels at low Z in our present calculation are in good agreement with experiments, and we expect that our results should be at least as accurate at high Z, because the wave functions will then be dominated by configurations within the same complex.[14]

In Table I, we list the energy levels and the corresponding configurations that we consider in this work. Spectroscopic notations are used for these states, though this is no more than a convenience in labeling the energy levels in our present intermediate coupling calculations. Specifically, the nine states that we have studied are, in order of increasing energy at low Z: $^1S^e$, $^3P^o(J=0,1,2)$, $^1P^o$, $^1D^e$ and $^3P^e$ $(J=0,1,2)$. For the sake of simplicity, the symbols p_+, p_-, d_+, and d_- are used to denote the $p_{3/2}$, $p_{1/2}$, $d_{5/2}$, and $d_{3/2}$ orbitals, respectively, in Table I and throughout this work, while p and d simply refer to the nonrelativistic designations of the orbitals with $l=1,2$, respectively.

B. Transition rates

For electromagnetic multipole transitions, the vector potential $\vec{A}(\vec{r})$ is expanded into a series of multipole vectors $\vec{a}_{JM}^{(\lambda)}(\vec{r})$, where $\lambda=1$ (0) denotes an electric (magnetic) multipole field and J, M are the angular momenta of the emitted photon. The transition rate $A_{i\to f}$ from an initial state $|jm\rangle$ to a final state $|j'm'\rangle$ by emission of a single photon is then given by

$$A_{i\to f} = 8\pi\alpha\omega \sum_{m'} |\langle j'm'|\vec{a}_{JM}^{(\lambda)}\cdot\vec{\alpha}|jm\rangle|^2. \quad (3)$$

Here, ω is the transition energy and $\vec{\alpha}$ is the usual Dirac matrix. Natural units are used in Eq. (3) and throughout this section. For electric multipole transitions, $\vec{a}_{JM}^{(1)}$ is given by

$$\vec{a}_{JM}^{(1)}(\vec{r}) = [(J+1)j_J(\omega r)/\omega r - j_{J+1}(\omega r)]\vec{Y}_{JM}^{(1)}(\hat{r}) + [J(J+1)]^{1/2}[j_J(\omega r)/\omega r]\vec{Y}_{JM}^{(-1)}(\hat{r}), \quad (4)$$

where $j_J(\omega r)$ is the spherical Bessel function of order J, and $\vec{Y}_{JM}^{(1)}$ and $\vec{Y}_{JM}^{(-1)}$ are vector spherical harmonics.

The expression of the vector field $\vec{a}_{JM}^{(1)}$ in Eq. (4) is based on an expansion of the vector potential $\vec{A}(\vec{r})$ in the Coulomb gauge.[15] In principle, a gauge transformation can always be made without affecting the transition matrix element $\langle j'm'|\vec{a}_{JM}^{(1)}\cdot\vec{\alpha}|jm\rangle$. In practice, however, it is well known that in approximate Hartree-Fock or MCHF calculations, the transition matrix is gauge dependent. In particular, the expression of $\vec{a}_{JM}^{(1)}$ in Eq. (4) reduces to the velocity form in the nonrelativistic limit, while a suitable gauge transformation can lead to the relativistic length form, with the subsequent replacement of the transition operator $\vec{a}_{JM}^{(1)}\cdot\vec{\alpha}$ by $\vec{a}_{JM}\cdot\vec{\alpha} - \phi_{JM}^*$, where[16]

$$\vec{a}_{JM} = -j_{J+1}(\omega r)\{\vec{Y}_{JM}^{(1)} - [(J+1)/J]^{1/2}\vec{Y}_{JM}^{(-1)}\},$$
$$\phi_{JM} = -i[(J+1)/J]^{1/2}j_J(\omega r)Y_{JM}. \quad (5)$$

Since gauge invariance is a fundamental physical constraint, the difference between the results of these two forms should provide a guide to the re-

liability of our present MCHF studies. For comparison purposes, we have calculated the transition matrix in both the length and the velocity forms. In doing so, we have taken into account a special feature of the MCHF calculations, specifically, the initial- and the final-state orbitals are not identical. A consequence of this is that when evaluating transition matrix elements, there will, in general, be "direct overlap" terms connecting identical single-particle orbitals in the initial and the final states, as well as "exchange overlap" terms arising from the nonzero overlaps of orbitals from different shells having the same angular symmetries. Detailed evaluation of the transition matrix elements involving nonorthogonal basis sets is given by Löwdin.[17]

As an immediate example, consider the transition from the $^1P^o$ state to the $^1S^e$ ground state. For simplicity, these two states are represented by single-configuration wave functions $|(3s3p_+)^1P\rangle$ and $|(3s^2)^1S\rangle$, as defined in Eq. (2). Let T be the transition operator, we then have

$$\begin{aligned}\langle(3s^2)^1S\,|\,T\,|\,(3s3p_+)^1P\rangle = {}& \langle 1s2s3s\,|\,1s2s3s\rangle\langle 2p_-\,|\,2p_-\rangle^2\langle 2p_+\,|\,2p_+\rangle^3 \\ & \times\{\langle 1s2s\,|\,1s2s\rangle[\langle 2p_+\,|\,2p_+\rangle\langle 3s\,|\,T\,|\,3p_+\rangle - \langle 2p_+\,|\,3p_+\rangle\langle 3s\,|\,T\,|\,2p_+\rangle] \\ & + \langle 3s1s\,|\,1s2s\rangle[\langle 2p_+\,|\,2p_+\rangle\langle 2s\,|\,T\,|\,3p_+\rangle - \langle 2p_+\,|\,3p_+\rangle\langle 2s\,|\,T\,|\,2p_+\rangle] \\ & + \langle 2s3s\,|\,1s2s\rangle[\langle 2p_+\,|\,2p_+\rangle\langle 1s\,|\,T\,|\,3p_+\rangle - \langle 2p_+\,|\,3p_+\rangle\langle 1s\,|\,T\,|\,2p_+\rangle]\}. \end{aligned} \tag{6}$$

Here, $\langle a\,|\,b\rangle$ is the overlap matrix element between orbitals a and b in the initial and the final states, respectively, and $\langle a_1, a_2, \ldots a_N\,|\,b_1, b_2, \ldots b_N\rangle$ is the determinant of an $N\times N$ matrix with $\langle a_i\,|\,b_j\rangle$ as its elements. For simplicity, the Clebsch-Gordan coefficients are absorbed into the one-particle transition matrix element $\langle a\,|\,T\,|\,b\rangle$. In the above expression, the direct overlap term is given by

$$\langle 1s\,|\,1s\rangle^2\langle 2s\,|\,2s\rangle^2\langle 2p_-\,|\,2p_-\rangle^2 \times \langle 2p_+\,|\,2p_+\rangle^4\langle 3s\,|\,3s\rangle\langle 3s\,|\,T\,|\,3p_+\rangle, \tag{7}$$

while the remaining terms in Eq. (6) are exchange overlap terms.

From this example, we can see that the inclusion of these exchange overlap terms will greatly complicate the calcuation, especially when multiconfiguration wave functions are used. However, as pointed out in Ref. 6, neglecting these terms may lead to anomalous results, especially in velocity form studies. In order to make a reliable comparison between the length and velocity calculations, a computer program was written to include these exchanges overlap terms in calculating various transitions.

TABLE II. Energy levels (in a.u.) of the Mg sequence relative to the ground state $^1S_0$.

Notation	$^3P^o$			$^1P^o$	$^1D^e$	$^3P^e$		
J=	0	1	2	1	2	0	1	2
Cl^{+5}	0.4420	0.4448	0.4499	0.6920	1.040	1.072	1.075	1.080
Expt.[a]	0.4472	0.4497	0.4550	0.6787	1.044[b]	1.071	1.074	1.079
Ca^{+8}	0.6484	0.6554	0.6699	0.9951	1.531	1.555	1.564	1.580
Expt.[c]	0.6452	0.6521	0.6668	0.9773	1.532	1.542	1.551	1.567
Fe^{+14}	1.065	1.092	1.155	1.628	2.558	2.543	2.587	2.664
Expt.[d]	1.066	1.092	1.157	1.604	2.550	2.527	2.572	2.650
Zn^{+18}	1.347	1.399	1.536	2.095	3.302	3.224	3.332	3.498
Kr^{+24}	1.784	1.890	2.244	2.918[e]	4.571	4.284	4.602	5.012
Mo^{+30}	2.241	2.416	3.199	3.975[f]	6.110	5.391	6.143	6.971
Cd^{+36}	2.724	2.977	4.516	5.393	8.044	6.557	8.079	9.217
Xe^{+42}	3.242	3.574	6.343	7.326	10.53	7.795	10.56	11.86
Gd^{+52}	4.206	4.671	11.05	12.22	16.43	10.08	16.48	17.98
W^{+62}	5.347	5.945	18.91	20.29	25.65	12.73	25.74	27.34
Pb^{+70}	6.438	7.144	28.65	30.21	36.61	15.23	36.80	38.38
U^{+80}	8.125	8.972	47.40	49.20	57.09	19.03	57.54	58.96

[a] Moore, Ref. 18.
[b] Victor *et al.*, Ref. 12.
[c] Ekberg, Ref. 19.
[d] Cowan and Widing, Ref. 20.
[e] $E_{expt} = 2.87$; Hinnov, Ref. 2.
[f] $E_{expt} = 3.89$; Hinnov, Ref. 2.

III. RESULTS AND DISCUSSIONS

In Table II, we list the values of the excitation energies from the ground state $^1S^e$ of all the low-lying energy levels considered in this work, together with available experimental results for comparison purposes. The systematic trends of these low-lying states along the isoelectronic sequences are depicted in Fig. 1. A noticeable effect is the change from the LS to the jj coupling schemes. At high Z, the energy levels are arranged in the order of $(j,j')=(\frac{1}{2},\frac{1}{2})$, $(\frac{1}{2},\frac{3}{2})$, $(\frac{1}{2},\frac{5}{2})$, $(\frac{3}{2},\frac{3}{2})$, ..., etc. As a consequence, some energy levels of the ground-state complex which lie high in the spectrum at low Z must come down and cross other states as Z increases. An example of such a level crossing is given in Fig. 1, where the $^3P^e_o$ state crosses $^1D^e_2$ at $Z\simeq 25$, $^1P^o_2$ at $Z\simeq 56$, and $^3P^o_2$ at $Z\simeq 62$ before it reaches its asymptotic position in the spectrum. Later, we shall return to the problem of level crossings and discuss their influence on the associated line strengths.

In Fig. 2, we list all the possible electric dipole transitions between the low-lying states considered in this work. The first eight lines shown to the left in Fig. 2 represent allowed transitions, while the rest are nonrelativistically forbidden ones.

In Table III, we give the values of the transition

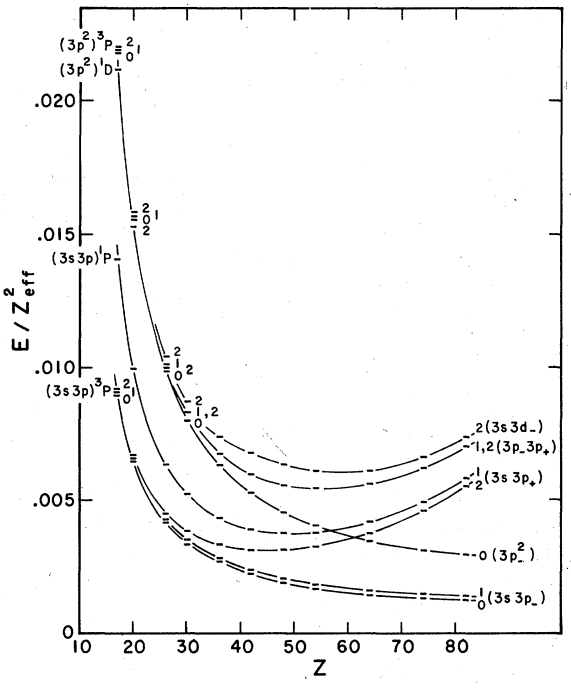

FIG. 1. Systematic trends of the low-lying energy levels in the Mg sequence. In this diagram, E is the excitation energy (a.u.) from the ground state $^1S^e$, and $Z_{eff}=Z-10$.

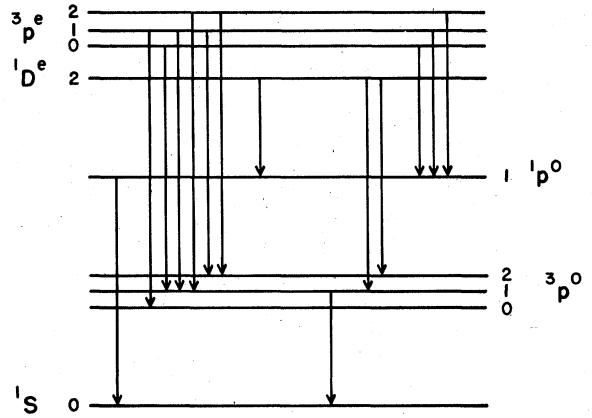

FIG. 2. $E1$ transitions considered in this work. The eight lines shown to the left in this diagram are allowed transitions, while the other six lines are forbidden ones.

energy ω and the values of the scaled line strengths Z^2S in both the length and the velocity forms (denoted by Z^2S_L and Z^2S_V, respectively) for the allowed transitions. Similar quantities for the forbidden ones are given in Table IV. One can see from these two tables that S_L and S_V are consistently in good agreement for all cases considered. Furthermore, one notices that S_L and S_V tend to agree better as Z increases, reflecting the diminishing importance of electron-electron correlations compared to the central nuclear potential. Large discrepancies between S_L and S_V arise only when there are severe cancellations in the transition matrices, as in the case of $^1P^o_1$-$^3P^e_o$ transitions.

In Figs. 3–6, the scaled line strengths Z^2S (length form only) are plotted as functions of Z for all the transitions considered. Since Z^2S is directly related to the scaled dipole transition matrix element, the decrease of Z^2S along the isoelectronic sequence for allowed transitions reflects the contractions of the orbitals due to relativistic effects. On the other hand, most of the forbidden transitions become comparable to the allowed ones at high Z because of the gradual transition from LS to jj couplings.

At this point, we would like to return to the problem of level crossings and their effects on the corresponding line strengths. In general, when level crossings occur for state characterized by the same set of quantum numbers J and π, there will be strong configuration mixing between these states. In such cases, the "normal" channels for transitions of these interacting states will be strongly perturbed, resulting in irregularities in the associated line strengths.

As an example, consider the first few low-lying states of even parity and $J=2$. At low Z, we iden-

TABLE III. Values of the allowed $E1$ transitions of the Mg sequence. For each transition, we list first the transition energies, followed by the scaled line strengths, Z^2S_L and Z^2S_V, respectively. All entries are in a.u.

$(j\text{-}j')$	Cl^{+5}	Ca^{+8}	Fe^{+14}	Zn^{+18}	Kr^{+24}	Mo^{+30}	Cd^{+36}	Xe^{+42}	Gd^{+52}	W^{+62}	Pb^{+70}	U^{+80}
						$^1S^e\text{-}^1P^o$						
(0-1)	0.6920	0.9951	1.628	2.095	2.917	3.975	5.393	7.326	12.22	20.29	30.21	49.20
	839	662	509	457	402	359	326	300	269	248	234	217
	829	661	514	462	407	364	330	303	271	249	234	217
						$^1P^o\text{-}^1D^e$						
(1-2)	0.3475	0.5360	0.9293	1.207	1.654	2.136	2.651	3.202	4.208	5.362	6.404	7.890
	432	398	288	235	181	143	118	102	87	78	70	55
	387	363	266	218	167	133	110	95	82	73	66	52
						$^3P^o\text{-}^3P^e$						
(0-1)	0.6325	0.9151	1.523	1.985	2.818	3.903	5.355	7.322	12.28	20.40	30.36	49.41
	311	247	192	173	156	145	137	131	123	116	109	96
	315	252	196	177	159	148	139	133	124	116	109	96
(1-0)	0.6268	0.8996	1.451	1.825	2.394	2.975	3.580	4.222	5.406	6.786	8.086	10.06
	310	246	189	170	153	144	138	134	126	118	112	103
	314	251	194	175	158	149	143	137	128	118	110	98
(1-1)	0.6297	0.9081	1.496	1.933	2.713	3.727	5.102	6.900	11.81	19.80	29.66	48.56
	233	185	143	128	112	99	89	82	72	66	63	61
	236	189	146	131	115	102	91	83	73	66	63	61
(1-2)	0.6351	0.9242	1.573	2.099	3.122	4.555	6.240	8.283	13.30	21.39	31.23	49.99
	384	293	186	147	118	164	317	308	330	356	377	401
	389	298	189	149	120	168	326	315	337	363	383	406
(2-1)	0.6246	0.8936	1.432	1.797	2.358	2.945	3.563	4.221	5.432	6.836	8.151	10.13
	387	307	237	213	190	175	164	155	143	132	124	114
	393	314	243	219	196	180	168	158	145	132	123	112
(2-2)	0.6300	0.9097	1.509	1.962	2.768	3.773	4.701	5.514	6.925	8.428	9.727	11.56
	1154	887	602	505	419	292	2.4	10.8	7.5	3.0	0.6	0.6
	1169	904	618	519	429	298	2.8	11.6	8.0	3.2	0.7	0.5

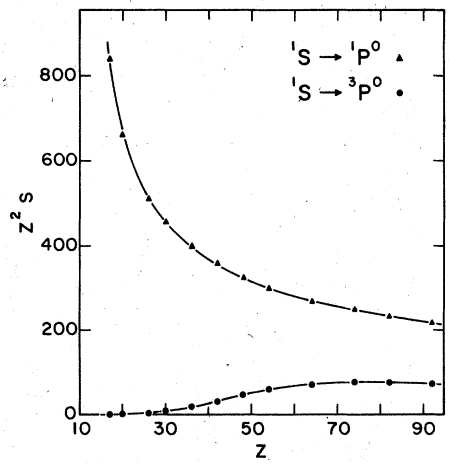

FIG. 3. Systematic trends of the scaled line strength Z^2S in the Mg sequence ($^1S \rightarrow {}^{1,3}P^o$).

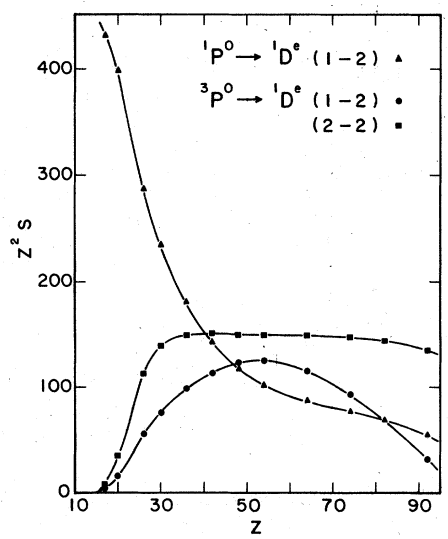

FIG. 4. Same as in Fig. 3, but for $^{1,3}P^o \rightarrow {}^1D^e$.

TABLE IV. Values of the forbidden $E1$ transitions of the Mg sequence. For each transition, we list first the transition energies, followed by the scaled line strengths Z^2S_L and Z^2S_V, respectively. All entries are in a.u.

$(j\text{-}j')$	Cl^{+5}	Ca^{+8}	Fe^{+14}	Zn^{+18}	Kr^{+24}	Mo^{+30}	Cd^{+36}	Xe^{+42}	Gd^{+52}	W^{+62}	Pb^{+70}	U^{+80}
						$^1S^e\text{-}^3P^o$						
(0-1)	0.4448	0.6554	1.092	1.399	1.890	2.417	2.977	3.575	4.671	5.949	7.144	8.972
	0.18	0.55	3.0	7.1	18.1	32.9	48.1	60.0	71.5	75.6	75.7	73.1
	0.22	0.61	3.3	7.7	19.4	34.7	50.9	62.8	73.8	76.6	75.6	71.5
						$^3P^o\text{-}^1D^e$						
(1-2)	0.5947	0.8757	1.466	1.904	2.682	3.694	5.067	6.952	11.76	19.70	29.47	48.12
	3.8	16.1	56.0	76.3	98.7	114	124	125	116	94.1	69.5	32.0
	3.9	16.3	56.6	77.0	99.4	115	124	125	115	93.3	68.9	31.6
(2-2)	0.5896	0.8612	1.402	1.767	2.327	2.912	3.528	4.183	5.381	6.740	7.966	9.688
	7.8	34.9	113	139	150	152	151	151	150	148	145	136
	7.8	35.6	117	143	155	157	156	154	152	148	144	135
						$^1P^o\text{-}^3P^e$						
(1-0)	0.3796	0.5599	0.9142	1.129	1.366	1.417	1.163	4.710	2.146[a]	7.556	14.98	30.17
	0.24	0.65	2.6	4.3	5.8	5.3	3.9	2.8	1.6	0.95	0.66	0.43
	0.30	0.84	3.4	5.8	8.1	8.1	7.6	13.5	6.3	0.71	0.56	0.39
(1-1)	0.3825	0.5684	0.9590	1.237	1.685	2.169	2.685	3.239	4.259	5.458	6.589	8.336
	0.04	0.15	0.88	2.1	5.2	9.5	13.7	17.0	20.1	21.2	21.3	21.6
	0.04	0.15	0.90	2.1	5.4	9.8	14.1	17.4	20.4	21.2	21.0	20.3
(1-2)	0.3879	0.5845	1.036	1.402	2.095	2.997	3.824	4.533	5.752	7.050	8.165	9.759
	4.9	20.2	65.0	79.8	76.4	44.5	4.6	0.36	2.0	9.5	17.7	30.9
	4.8	17.3	57.0	71.5	69.9	41.0	5.1	0.56	1.6	8.6	16.6	29.5

[a]The direction of transition is inverted because of the level crossing of $^1P^o_1$ and $^3P^e_0$.

tify the second eigenstate with these quantum numbers as the $(3p^2_{3/2})^3P^e_2$ state, while the third one is the $(3s3d_{3/2})^3D^e_2$ state. Since the $(3s3d_{3/2})_{J=2}$ state is lower in energy than the $(3p^2_{3/2})_{J=2}$ state in the jj coupling limit, these two states must cross at some intermediate Z.

In Fig. 7, the systematic trends of the first four eigenstates with even parity and $J=2$ are shown.

As we can see, the crossing of the $(3s3d_{3/2})_{J=2}$ and the $(3p^2_{3/2})_{J=2}$ states occurs at $Z \simeq 45$. If we compared this diagram with Fig. 7 where the scaled line strengths of the three transitions originating from the $^3P^e_2$ state are plotted, we can see that the irregularities of the Z^2S curves indeed

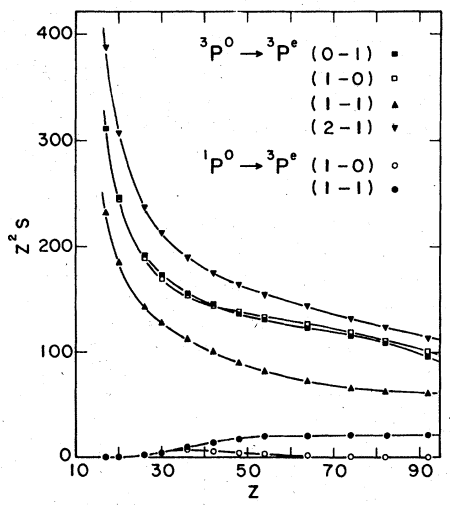

FIG. 5. Same as in Fig. 3, but for $^{1,3}P^o \rightarrow {}^3P^e$.

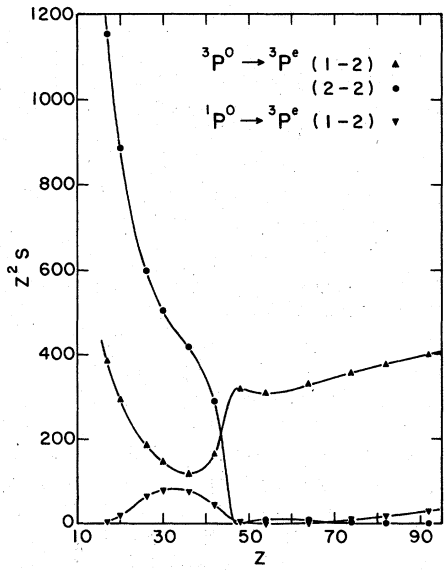

FIG. 6. Same as in Fig. 3, but for $^{1,3}P^o \rightarrow {}^3P^e$.

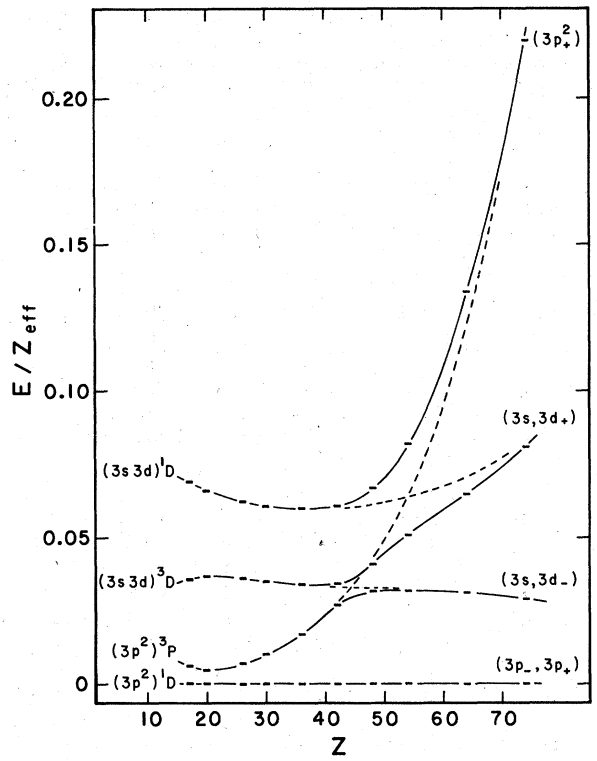

FIG. 7. Systematic trends of the first four eigenstates with even parity and $J=2$. In this diagram, E is the energy (a.u.) relative to the lowest eigenstate $^1D^e_2$, and $Z_{\text{eff}}=Z-10$.

arise in the same region where the interaction between the $(3s3d_{3/2})$ and the $(3p^2_{3/2})$ configurations are the strongest. Furthermore, destructive interference between transition channels arising from the mixing of the $(3p^2)$ and $(3s3d)$ configurations in $^3P^e_2$ state strongly suppresses the transitions $^3P^o_2$-$^3P^e_2$ and $^1P^o_1$-$^3P^e_2$ in the high Z region, while the transition $^3P^o_1$-$^3P^e_2$ is enhanced by the coherent mixing of the asymptotic configurations.

At the beginning of this section, we pointed out crossings of the $^3P^e_o$ state with the $^1D^e_2$, $^1P^o_1$, and $^3P^o_2$ states. These crossings, however, are less interesting because the various states involved are characterized by different sets of quantum numbers J and π and so they cannot interact with each other. The sole effect of these level crossings is the inversion of the direction of the $^1P^e_1$-$^3P^e_o$ transition. However, since this transition is forbidden in both the LS and jj limit, the effect of this level crossing is not at all obvious when we look at the corresponding graph in Fig. 5.

At any rate, level crossings involving strongly interacting states are so common that we should not expect that the irregularities in the line strengths in our former example represent isolated phenomena. In establishing the systematic trends for the S values, it is therefore important to take particular care of the regions of possible crossing anomalies. In this respect, the present relativistic MCHF scheme is especially suitable for the studies of level crossings, because both intermediate coupling and relativistic effects are included in calculating the energy levels along an isoelectronic sequence.

TABLE V. Improvement of excitation energies (a.u.) and oscillator strengths for the resonance transition $^1S^e$-$^1P^o$ of the Mg sequence when additional configurations are included in the calculation. For each ion, the first line corresponds to results without the $3d$ configurations, while the second line gives results with $3d$ configurations included exactly.

Ion	ω	ω_{expt} [a]	f_L	f_V
Mg	0.2182		1.75	0.90
	0.1608	0.1597	1.73	1.79
P^{+3}	0.5371		1.65	1.38
	0.4890	0.4793	1.57	1.53
Ar^{+6}	0.8547		1.29	1.13
	0.7928	0.7779	1.25	1.24
Fe^{+14}	1.716		0.839	0.763
	1.628	1.604 [b]	0.818	0.825
Kr^{+24}	3.025		0.617	0.578
	2.917	2.87 [c]	0.603	0.611
Xe^{+42}	7.437		0.510	0.496
	7.326		0.502	0.507
U^{+80}	49.29		0.841	0.835
	49.20		0.842	0.841

[a] Moore, Ref. 18.
[b] Cowan and Widing, Ref. 20.
[c] Hinnov, Ref. 2.

IV. CONCLUSION

It is well known that configurations involving $3d$ electrons play an important role in the low-lying states of Mg-like ions. To show the effects of these configurations, we list in Table V some energies and oscillator strengths for the transition $^1S^e$-$^1P^o$ calculated with and without the $3d$ configura-

TABLE VI. Comparison of the calculated oscillator strengths for several allowed transitions of the Cl^{+5} ion with the model potential calculations of Ref. 12.

Transition	This work	Model potential	Experiment
$^1S^e$-$^1P^o$	1.34	1.27	0.97 [a]
$^1P^o$-$^1D^e$	0.115	0.116	0.14 [b]
$^3P^o$-$^3P^e$	0.449 [c]	0.430	0.35 [b]

[a] Bashkin and Martinson, Ref. 21.
[b] Bashkin, *et al.*, Ref. 22.
[c] Multiplet averaged value.

TABLE VII. Comparison of the present values of excitation energies and oscillator strengths for the resonance transition $^1S^e$-$^1P^o$ with other theoretical and experimental values along the Mg sequence.

Ion	ω (a.u.)			Oscillator strengths				
	MCHF	RRPA [a]	Expt. [j]	MCHF	RRPA [a]	NBS [b]	M.P. [c]	Others
Mg	0.1608	0.1496	0.1597	1.73	1.67	1.81	1.72	1.66 [d]; 1.71 [e]; 1.76 [f,g,h]; 1.86 [m]; 1.9 [n]; 1.80 [p]; 1.85 [q]; 1.75 [r]; 1.67 [s]; 2.4 [t]
Al^{+1}	0.2789	0.2667	0.2727	1.85	1.85	1.84	1.77	1.8 [n]; 1.9 [t]
Si^{+2}	0.3855	0.3745	0.3776	1.71	1.73	1.70	1.62	1.7 [u]; 1.6 [v]
P^{+3}	0.4890	0.4782	0.4793	1.57	1.59	1.60	1.48	1.8 [w]; 1.2 [x]
S^{+4}	0.5909	0.5796	0.5797	1.45	1.47	1.46	1.36	1.06 [y]; 1.6 [z]; 0.24 [aa]; 1.03 [bb]
Cl^{+5}	0.6920	0.6799	0.6787	1.34	1.36	1.28	1.27	0.97 [cc]
Ar^{+6}	0.7928	0.7798	0.7779	1.25	1.27	1.21		0.84 [bb]; 0.86 [dd]
Ca^{+8}	0.9950	0.9798	0.9773	1.10	1.11	1.09		
Fe^{+14}	1.628	1.605	1.604 [k]	0.818	0.827			0.83 [i]
Kr^{+24}	2.917	2.880	2.87 [l]	0.603	0.611			
Mo^{+30}	3.975	3.927	3.89 [l]	0.540	0.549			
Xe^{+42}	7.326	7.260		0.502	0.509			
W^{+62}	20.29	20.21		0.612	0.616			
U^{+80}	49.20	49.14		0.842	0.843			

Theories:
[a] Shorer *et al.*, Ref. 9.
[b] Wiese *et al.*, Ref. 23 (based on Refs. 24, 25, 26).
[c] Model potential calculations of Victor *et al.*, Ref. 12.
[d] Amusia and Cherepkov, Ref. 27.
[e] Kim and Bagus, Ref. 28.
[f] Fischer, Ref. 29.
[g] Bates and Altick, Ref. 30.
[h] Saraph, Ref. 31.
[i] Cowan and Widing, Ref. 20.

Experiments:
[j] Moore, Ref. 18.
[k] Cowan and Widing, Ref. 20.
[l] Hinnov, Ref. 2.
[m] Smith and Liszt, Ref. 32.
[n] Smith, Ref. 33.
[p] Smith and Gallagher, Ref. 34.
[q] Lurio, Ref. 35.

Beam-foil experiments:
[r] Lundin *et al.*, Ref. 36.
[s] Andersen *et al.*, Ref. 37.
[t] Berry *et al.*, Ref. 38.
[u] Berry *et al.*, Ref. 39.
[v] Irwin and Livingston, Ref. 40.
[w] Curtis *et al.*, Ref. 41.
[x] Livingston *et al.*, Ref. 42.
[y] Irwin and Livingston, Ref. 43.
[z] Based on unpublished results of T. Anderson and G. Sørensen quoted in Ref. 44.
[aa] Berry *et al.*, Ref. 45.
[bb] Irwin *et al.*, Ref. 46.
[cc] Bashkin and Martinson, Ref. 21.
[dd] Livingston *et al.*, Ref. 47.

tions. Both the length and the velocity form oscillator strengths (f_L and f_V) are presented for comparison purposes.

At low Z, where the $3d$ electron correlations are most important, there is, in general, a large discrepancy between f_L and f_V when the $3d$ configurations are omitted, and the transition energies ω are not in good agreement with experiment under this circumstance. By including $3d$ configurations in the calculations, the agreement between ω and ω_{expt} is greatly improved, as well as the agreement between f_L and f_V. This situation changes gradually, however, as Z increases. At high Z, the values of transition energies and oscillator strengths are only slightly modified by the inclusion of the $3d$ configurations, reflecting the diminishing role of correlation effects in the asymptotic region. The close agreement between f_L and f_V in our present work thus serves not only as a measure of the reliability of the MCHF scheme, but also as an indication of the adequacy of the configurations included in the calculations.

From Table V, we further notice that f_V is, in general, more sensitive to the inclusion of the $3d$ configurations, while f_L does not change appreciably throughout the entire sequence. This observation suggests that the length form is to be preferred in the present MCHF calculations, at least when there are no severe cancellations in evaluating the length form transition matrix elements.

Our results on the systematic trends of line strengths along the sequence for all transitions considered are in qualitative agreement with the recent SOC study of Wiess.[11] In Table VI, we compare quantitatively the f values of several allowed transitions for the Cl^{+5} ion with recent model potential calculations of Victor, Stewart, and Laughlin[12] and with experiments. Despite the relatively few configurations included in the wave functions of the present MCHF calculations, our results are

consistent with the model potential calculations for the transitions considered. Since the low-lying states are dominated by configurations of the ground-state complex in the jj coupling limit, we therefore expect that our results should be at least as accurate in the intermediate and high-Z regions.

In Table VII, excitation energies ω and oscillator strengths f_L of the present calculations for the resonance transition $^1S^e$-$^1P^o$ are compared with other theories and with experiments along the sequence. For neutral magnesium and other low-Z ions, our results are consistent with other studies. Since we have confined our attention to the configurations within the same complex, it appears that intercomplex interactions are small in the Mg sequence, even at low Z, where the correlation effects are the strongest, in accordance with the observations in Ref. 10. At high Z, the close agreement between the present work and the RRPA calculations illustrates the appropriateness of either technique in dealing with the properties of highly stripped atomic systems.

In this work, we have demonstrated the utility of the relativistic MCHF scheme by presenting results of our calculations on the excitation energies and line strengths of the Mg sequence. From the results of this work, it appears that the present relativistic MCHF scheme is a powerful technique in establishing the systematic trends of the low-lying states, as well as the line strengths throughout the entire sequence, even near regions with crossing anomalies.

ACKNOWLEDGMENTS

The authors are indebted to A. W. Weiss for communicating his data on the Mg sequence prior to publication. Our MCHF orbitals were determined numerically, using a computer code developed by J. P. Desclaux.[48] We thank Y. K. Kim and D. L. Lin for advice on implementing the Desclaux code.

---

*Work supported in part by NSF Grant No. GP-42738.

†Present address: Argonne National Laboratory, Argonne, Ill. 60439.

[1]A. H. Gabriel and C. Jordan, Case Stud. At. Coll. Phys. 2, 211 (1972).
[2]E. Hinnov, Phys. Rev. A 14, 1533 (1976).
[3]I. Martinson and A. Gaupp, Phys. Rep. 15C, 113 (1974).
[4]Y. K. Kim and J. P. Desclaux, Phys. Rev. Lett. 36, 139 (1976).
[5]L. Armstrong, Jr., W. R. Fielder, and D. L. Lin, Phys. Rev. A 14, 1114 (1976).
[6]K. T. Cheng and W. R. Johnson, Phys. Rev. A 15, 1326 (1977).
[7]W. R. Johnson and C. D. Lin, Phys. Rev. A 14, 565 (1976); W. R. Johnson, C. D. Lin, and A. Dalgarno, J. Phys. B 9, L303 (1976); C. D. Lin, W. R. Johnson, and A. Dalgarno, Phys. Rev. A 15, 154 (1977).
[8]C. D. Lin and W. R. Johnson, Phys. Rev. A 15, 1046 (1977).
[9]P. Shorer, C. D. Lin, and W. R. Johnson, unpublished.
[10]M. Aymar and E. Luc-Koenig, Phys. Rev. A 15, 821 (1977).
[11]A. W. Weiss (private communication).
[12]G. A. Victor, R. F. Stewart, and C. Laughlin, Astrophys. J. Suppl. Ser. 31, 237 (1976).
[13]R. F. Stewart, Mol. Phys. 30, 745 (1975).
[14]D. Layzer, Ann. Phys. (N.Y.) 8, 271 (1959).
[15]A. I. Akhiezer and V. B. Berestetskii, *Quantum Electrodynamics* (Interscience, New York, 1965).
[16]I. P. Grant, J. Phys. B 7, 1458 (1974).
[17]P. O. Löwdin, Phys. Rev. 97, 1474 (1955).
[18]C. E. Moore, *Atomic Energy Levels*, Natl. Bur. Stand. Circ. (U.S. GPO, Washington, D. C., 1949), Vol. I.
[19]J. O. Ekberg, Phys. Scr. 4, 101 (1971).
[20]R. D. Cowan and K. G. Widing, Astrophys. J. 180, 285 (1973).
[21]S. Bashkin and I. Martinson, J. Opt. Soc. Am. 61, 1686 (1971).
[22]S. Bashkin, J. Bromander, J. A. Leavitt, and I. Martinson, Phys. Scr. 8, 285 (1973).
[23]W. L. Wiese, M. W. Smith, and B. M. Miles, *Atomic Transition Probabilities*, NSRDS-NBS 22 (U.S. GPO, Washington, D. C., 1969), Vol. II.
[24]A. W. Weiss, J. Chem. Phys. 47, 3573 (1967).
[25]R. N. Zare, J. Chem. Phys. 47, 3561 (1967).
[26]R. J. S. Crossley and A. Dalgarno, Proc. R. Soc. Lond. A 286, 510 (1965).
[27]M. Ya. Amusia and N. A. Cherepkov, Case Stud. At. Phys. 5, 47 (1975).
[28]Y. K. Kim and P. S. Bagus, J. Phys. B 5, L193 (1972).
[29]C. F. Fischer, Can. J. Phys. 53, 338 (1975).
[30]G. N. Bates and P. L. Altick, J. Phys. B 6, 653 (1973).
[31]H. E. Saraph, J. Phys. B 9, 2379 (1976).
[32]W. H. Smith and H. S. Liszt, J. Opt. Soc. Am. 61, 938 (1971).
[33]W. H. Smith, Nucl. Instrum. Methods 90, 115 (1970).
[34]W. W. Smith and A. Gallagher, Phys. Rev. 145, 26 (1966).
[35]A. Lurio, Phys. Rev. 136, A376 (1964).
[36]L. Lundin, B. Engman, J. Hilke, and I. Martinson, Phys. Scr. 8, 274 (1973).
[37]T. Andersen, J. Desesquelles, K. A. Jessen, and G. Sørensen, J. Quant. Spectrosc. Radiat. Transfer 10, 1143 (1970).
[38]H. G. Berry, J. Bromander, and R. Buchta, Phys. Scr. 1, 181 (1970).
[39]H. G. Berry, J. Bromander, L. J. Curtis, and R. Buchta, Phys. Scr. 3, 125 (1971).
[40]D. J. G. Irwin and A. E. Livingston, Can. J. Phys. 51, 848 (1973).
[41]L. J. Curtis, I. Martinson, and R. Buchta, Phys.

Scr. 3, 197 (1971).
[42]A. E. Livingston, J. A. Kernahan, D. J. G. Irwin, and E. H. Pinnington, Phys. Scr. 12, 223 (1975).
[43]D. J. G. Irwin and A. E. Livingston, Can. J. Phys. 54, 805 (1976).
[44]G. Sørensen, Phys. Rev. A 7, 85 (1973).
[45]H. G. Berry, R. M. Schectman, I. Martinson, W. S. Bickel, and S. Bashkin, J. Opt. Soc. Am. 60, 335 (1970).
[46]D. J. G. Irwin, A. E. Livingston, and J. A. Kernahan, Nucl. Instrum. Methods 110, 111 (1973).
[47]A. E. Livingston, D. J. G. Irwin, and E. H. Pinnington, J. Opt. Soc. Am. 62, 1303 (1972).
[48]J. P. Desclaux, Comput. Phys. Commun. 9, 31 (1975).